Design Project: Phase One

Jarod Tang

August 2024

Contents

1 Introduction **2**

2 Performance Requirements **2**

3 Project Tasks **2**

3.1 Sensor and Actuator Selection 2

3.1.1 Actuator Selection: 2

3.1.2 Sensor Selection: 4

3.2 Obtaining Linearised model 4

3.3 Performance Requirements for Linear Control Design 5

3.4 Intial Continuous-Time Controller Design 7

3.5 Digital Emulation of the Controller on the Linear Model 8

3.6 Implementation and Testing 10

3.6.1 Initial Implementation 10

3.6.2 Redesign and Implementation 11

4 Discussion **12**

5 Conclusion **12**

1 Introduction

The primary goal of phase 1 of this design project is to familarise with and develop a control system for a single-link flexible-joint robot system while ensuring it meets specified performance requirements. The control system is tasked with moving the arm repeatedly between 15° and 45° angular positions after 3 second intervals, where the arm's angle θ_l must track a square wave with a 15° amplitude, 30° offset, and a 6-second period. After selecting suitable sensors and actuators, a linear model of the plant and motor combination is designed. A continuous time controller is then designed using classical control design principles and subsequently emulated and evaluated on the nonlinear plant.

2 Performance Requirements

The performance requirements are as follows:

- Steady state error of at most 2 degrees for the arm angular position θ_l.
- Maximum magnitude of 5 degrees for any overshoot/undershoot of θ_l when the reference signal changes direction.
- Settling time of at most 2.0 seconds (for a less than 2% settling time).
- Maximum controller sampling frequency of 50 Hz.

3 Project Tasks

3.1 Sensor and Actuator Selection

3.1.1 Actuator Selection:

As specified in the Design Project document provided, the state space was chosen as such, where θ_m, θ_l, $\dot{\theta}_m$, $\dot{\theta}_m$ and I_a is the angular position of the motor and load with respect to the fixed base, angular speed of the motor and load and the armature current respectively.

$$\mathbf{x} = \begin{bmatrix} x_1 & x_2 & x_3 & x_4 & x_5 \end{bmatrix} = \begin{bmatrix} \theta_m & \theta_l & \dot{\theta}_m & \dot{\theta}_l & I_a \end{bmatrix} \tag{1}$$

The plant and motor model provided by the Design Project specifications is as follows and depicted by Equations 2 and 3 respectively. Note that K_s is the spring constant.

$$\begin{bmatrix} \dot{x}_1 \\ \dot{x}_2 \\ \dot{x}_3 \\ \dot{x}_4 \end{bmatrix} = \begin{bmatrix} 0 & 0 & 1 & 0 \\ 0 & 0 & 0 & 1 \\ -\frac{K_s}{J_m} & \frac{K_s}{J_m} & 0 & 0 \\ \frac{K_s}{J_l} & -\frac{K_s}{J_l} & 0 & 0 \end{bmatrix} \begin{bmatrix} x_1 \\ x_2 \\ x_3 \\ x_4 \end{bmatrix} + \begin{bmatrix} 0 \\ 0 \\ \frac{-b \cdot \mathrm{sgn}(x_3) x_3^2}{J_m} \\ \frac{mgl \sin(x_2)}{J_l} \end{bmatrix} + \begin{bmatrix} 0 \\ 0 \\ \frac{1}{J_m} \\ 0 \end{bmatrix} T_m \tag{2}$$

$$\dot{x}_5 = -\frac{R_a}{L_a}x_5 - \frac{K_m}{L_a}x_3 + \frac{1}{L_a}u \tag{3}$$

To find the required torque for a given steady-state specification, equilibrium analysis of both the plant and motor model was performed by setting all the derivative terms to 0. This yields the following plant state space model expressed by Equation 4 and the motor model expressed by Equation 5.

$$\begin{bmatrix}0\\0\\0\\0\end{bmatrix} = \begin{bmatrix}0 & 0 & 1 & 0\\ 0 & 0 & 0 & 1\\ \frac{K_s}{J_m} & \frac{K_s}{J_m} & 0 & 0\\ \frac{K_s}{J_l} & -\frac{K_s}{J_l} & 0 & 0\end{bmatrix}\begin{bmatrix}x_1\\x_2\\x_3\\x_4\end{bmatrix} + \begin{bmatrix}0\\0\\0\\\frac{-mgl\cdot\sin(x_2)}{J_l}\end{bmatrix} + \begin{bmatrix}0\\0\\\frac{1}{J_m}\\0\end{bmatrix} T_m \tag{4}$$

$$0 = -\frac{R_a}{L_a}x_5 - \frac{K_m}{L_a}x_3 + \frac{1}{L_a}u \tag{5}$$

Observing rows three and four of Equation 4, Equations 6 and 7 can be extracted. For clarity, the state space variables have been substituted for their actual values stated in Equation 1. Note that $T_m = K_m I_a$.

$$0 = K_s(\theta_l - \theta_m) - T_m \tag{6}$$

$$0 = -K_s(\theta_l - \theta_m) - mg\ell\sin(\theta_l) \tag{7}$$

For the system to be in stable equilibrium, θ_l must either be at 15°or 45°relative to the fixed base, since the system must hold the load at this position for a prolonged period of time. However, $\theta_l = 30°$ should also be considered, since this is the midpoint of aforementioned angular positions. The consideration of this value is discussed further in Section 3.2. These values of θ_l can be substituted into Equations 6 and 7 to derive θ_m and subsequently, the required torque to maintain these positions (T_m). The derived torque will serve as a minimum requirement that the motors must achieve. The spring constant $K_s \in [1.55, 1.80]$ was chosen to be 1.80. This choice of K_s serves as a safety factor as it will increase the value of T_m and subsequently the minimum required torque. The results are depicted in Table 1.

	$\theta_l = 45°$	$\theta_l = 15°$	$\theta_l = 30°$
θ_m (°)	47.21	15.81	31.56
T_m (Nm)	0.0694	0.0254	0.049

Table 1: Equilibrium Solutions

Based on the provided actuator specifications, Motors 1 and 2 meet the minimum torque requirement, while Motor 3 does not. In comparing Motors 1 and 2, several factors are worth considering. Motor 1 has a higher torque output, offering finer control. Additionally, it is more economical, since it is both cheaper and has a longer service life. Motor

2 while having lower torque, provides a significantly higher angular velocity, enabling it to respond faster to control signals. In addition, Motor 2 operates at a higher voltage, reducing its sensitivity to noise.

Whilst noting that Motor 1 remains a viable option for this task, Motor 2 was chosen for its fast response time and resilience to noise. Moreover, in the selection of this motor, there is less emphasis on longevity and cost savings as it is not an explicit requirement of the Design Project.

3.1.2 Sensor Selection:

In this process, only sensors that provided information about the load were considered since when deriving the linear model in Section 3.2, the state space variables pertaining to the motor are negated. Therefore, only the Vision and Gyroscope were considered.

In comparing these two sensors, the gyroscope directly measures the link's angular velocity, is capable of high sampling rates without loss of accuracy and is relatively cheap. However, since the velocity readings must be integrated, drift is introduced, which leads to cumulative errors in measurement. The vision sensors available can provide a direct measurement of the angular position, eliminating the need for integration and subsequent drift issues. The best vision sensor available operates at 100fps, offering sufficient sampling frequency to meet the system's requirements, however, is quite expensive at $416AUD. Even though the vision sensor is substantially more expensive than the gyroscope, the vision sensor is more suitable for the task given the performance requirements. Moreover, there is no budget or emphasis on economic value in the Design Project document.

3.2 Obtaining Linearised model

As per Section 3.1, K_s was set to 1.8. The value b represents the damping coefficient and lies between 0.013 and 0.019. As observed in Equation 13, this value will not carry over in the calculation of the linearised model and subsequently, selection of a b value is trivial . The nonlinear system model for the plant and motor combination is shown below in Equation 8.

$$\begin{bmatrix} \dot{x}_1 \\ \dot{x}_2 \\ \dot{x}_3 \\ \dot{x}_4 \\ \dot{x}_5 \end{bmatrix} = \begin{bmatrix} 0 & 0 & 1 & 0 & 0 \\ 0 & 0 & 0 & 1 & 0 \\ -\frac{K_s}{J_m} & \frac{K_s}{J_m} & 0 & 0 & \frac{K_m}{J_m} \\ \frac{K_s}{J_l} & -\frac{K_s}{J_l} & 0 & 0 & 0 \\ 0 & 0 & -\frac{K_m}{L_a} & 0 & -\frac{R_a}{L_a} \end{bmatrix} \begin{bmatrix} x_1 \\ x_2 \\ x_3 \\ x_4 \\ x_5 \end{bmatrix} + \begin{bmatrix} 0 \\ 0 \\ \frac{-b \cdot \mathrm{sgn}(x_3) x_3^2}{J_m} \\ \frac{mgl \sin(x_2)}{J_l} \\ \frac{1}{L_a} \mathrm{u} \end{bmatrix} \tag{8}$$

Taking the partial derivative of Equation 8 yields the below expression depicted by Equations 10 and 11, which takes the linearised form expressed by Equation 9.

$$\begin{aligned} \dot{x}(t) &= Ax(t) + Bu(t) \\ y(t) &= Cx(t) + Du(t) \end{aligned} \tag{9}$$

$$\frac{d\bar{x}}{dt} = \begin{bmatrix} 0 & 0 & 1 & 0 & 0 \\ 0 & 0 & 0 & 1 & 0 \\ -\frac{K_s}{J_m} & \frac{K_s}{J_m} & -\frac{2b|x_3*|}{J_m} & 0 & \frac{K_m}{J_m} \\ \frac{K_s}{J_l} & -\frac{K_s}{J_l} - \frac{mgl\cos(x_2*)}{J_l} & 0 & 0 & 0 \\ 0 & 0 & -\frac{K_m}{L_a} & 0 & -\frac{R_a}{L_a} \end{bmatrix} \bar{x} + \begin{bmatrix} 0 \\ 0 \\ 0 \\ 0 \\ \frac{1}{L_a} \end{bmatrix} \bar{u} \tag{10}$$

$$y(t) = \begin{bmatrix} 0 & 1 & 0 & 0 & 0 \end{bmatrix} \bar{x} \tag{11}$$

Linearisation approximates a nonlinear system around a specific operating point to derive a linear model. For choosing an equilibrium point, both $\theta_l = 15°$ and $\theta_l = 45°$ were considered. However, say for example if linearisation were to happen about $\theta_l = 15°$, then the linear model would provide a poor approximation about $\theta_l = 45°$ since the approximation would perform worse about points further away from the chosen equilibrium point and vice versa. Therefore, for this system, a linearisation point of $\theta_l = 30°$ was chosen, since this angular position is equidistant to both 15° and 45°. Additionally, a midpoint linearisation would provide a smoother transition between these two extremes, providing a balanced representation of the system's dynamics. The fixed equilibrium point is defined below by Equation 12. Note that x_5* was obtained by solving the relationship for T_m defined in Section 3.1 where $I_a = x_5*$

$$\begin{bmatrix} x_1* & x_2* & x_3* & x_4* & x_5* \end{bmatrix} = \begin{bmatrix} 31.56 & 30 & 0 & 0 & 1.8167 \end{bmatrix} \tag{12}$$

Substituting these values yields the following A and B matrices.

$$A = \begin{bmatrix} 0 & 0 & 1 & 0 & 0 \\ 0 & 0 & 0 & 1 & 0 \\ -240000 & 240000 & 0 & 0 & 3600 \\ 1800 & -1880 & 0 & 0 & 0 \\ 0 & 0 & -20.77 & 0 & -1539 \end{bmatrix} \tag{13}$$

$$B = \begin{bmatrix} 0 \\ 0 \\ 0 \\ 0 \\ 769.23 \end{bmatrix} \tag{14}$$

3.3 Performance Requirements for Linear Control Design

Using Equation 15, the linearised system model for the plant and motor combination transfer function can be obtained using Equation 16. Note that D = 0 in this context.

$$C \cdot (sI - A)^{-1} \cdot B + D \tag{15}$$

$$G(s) = \frac{4.99 \times 10^9}{s^5 + 1538.00s^4 + 3.17 \times 10^5 s^3 + 3.72 \times 10^8 s^2 + 1.61 \times 10^8 s + 3.14 \times 10^{10}} \tag{16}$$

Plotting the bode plot of the transfer function yields the following plots depicted by Figure 1. The observed gain and phase margin and the crossover frequency are listed in Table 2. Moreover, it can be ascertained that the linearised model is stable.

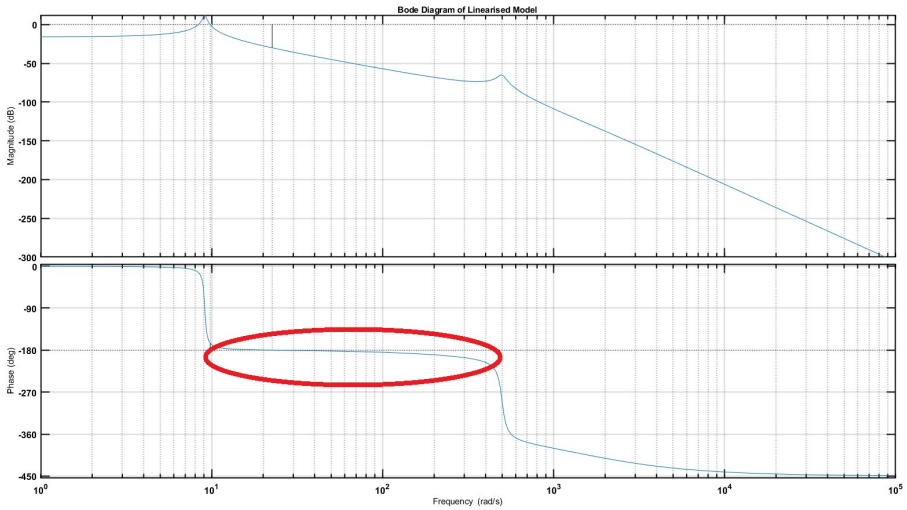


Figure 1: Plant Bode Plot

Using the specifications outlined in Section 2, the time-domain performance requirements can be converted to the frequency domain. Using Equations 17, the frequency requirements ζ (damping ratio), ω_n (natural freqeuncy), ω_c (cutoff-frequency) and M_f (phase margin) can be obtained. These values are listed in Table 3. However, as these high-level performance requirements are given for the nonlinear system, the controller should be designed about tighter requirements as not only does this create a more robust system, but also buffers for the inaccuracies and limitations of the linearised model. The tighter requirements are made by halving the performance specifications. The new requirements are listed in Table 4.

$$\begin{aligned} \zeta &= \sqrt{\frac{\left(\frac{-\ln(M_p)}{\pi}\right)^2}{\left(\frac{-\ln(M_p)}{\pi}\right)^2 + 1}} & \omega_n &= \frac{1}{-\zeta t_s} \ln\left(\frac{\delta}{100}\sqrt{1-\zeta^2}\right) \\ \omega_c &= \omega_n \sqrt{\sqrt{1+4\zeta^2} - 2\zeta^2} & M_f &= \arctan\left(\frac{2\zeta}{\sqrt{\sqrt{1+4\zeta^2} - 2\zeta^2}}\right) \end{aligned} \tag{17}$$

G_m	31.72
P_m	14.86
W_c	9.79

Table 2: Bode Plot Results

ζ	0.573
ω_n	3.59
ω_c	3.33
M_f	50.96

Table 3: Minimum Performance Requirements

ζ	0.677
ω_n	7.25
ω_c	6.35
M_f	57.12

Table 4: Tightened Requirements

As observed in Table 4, the lower bound on the cross-over frequency is $\omega_c = 6.35\,\text{rad/s}$. However, when observing the Bode plot depicted by Figure 1, there are two peaks present, occurring at $\omega_{\text{peak, 1}} = 9.11\,\text{rad/s}$ and $\omega_{\text{peak, 2}} = 498\,\text{rad/s}$. Since $\omega_{\text{peak, 1}} > 6.35$, $\omega_{c,\text{lower}}$ should be set to a value greater than $9.11\,\text{rad/s}$ to avoid the bode plot crossing over the 0dB line twice. This provides clearance of over $400 rad/s$ in selecting a ω_c in Section 3.4. Moreover, given that the distance along the frequency axis between these two peaks is quite large, a suitable cross-over frequency can be selected within this region, so long as its corresponding magnitude value is greater than the magnitude value associated with $\omega_{\text{peak, 2}}$. Furthermore, to reach the desired phase margin of at least $57.12°$, phase lead will be required.

3.4 Intial Continuous-Time Controller Design

As stated in Section 3.3, phase lead is required. Moreover, the lower bound of the cross-over frequency is set to $\omega_{c,\text{lower}} = 9.11 rad/s$. Observing Figure 1, this requirement can be interpreted as the need to push the area encircled in red up until at least the phase margin requirement is met. This can be achieved by using a controller. For this task, a PID controller was selected for the following reasons:

- PID controllers inherently provide the necessary phase lead to meet the phase margin requirements
- The presence of the derivative action helps to reduce overshoot and refine the transient response.
- Whilst a phase lead controller would improve phase margin, it does not address steady-state error and would require additional compensation.

The PID controller takes the causal form depicted by Equation 18 below. Note that this is an approximation of a typical PID controller, as that form cannot be implemented in practice as it is non-causal.

$$\tilde{C}(s) = \frac{K(\tau_{z_1}s+1)(\tau_{z_2}s+1)}{s(\tau_p s+1)} = \frac{1}{\tau_p s+1}\left(K(\tau_{z_1}+\tau_{z_2}) + \frac{K}{s} + K\tau_{z_1}\tau_{z_2}s\right) \tag{18}$$

In designing a suitable controller, loop shaping was employed as the primary technique to meet the performance requirements. This process involves iteratively tuning key parameters such as the crossover frequency (ω_c), phase margin (M_f), and the proportional

(K_p), integral K_i), and derivative (K_d) gains of the PID controller to shape the open-loop frequency response, such that the desired response is achieved. Additionally, given that Motor 2 operates at 12V, the controller output should be monitored to account for potential voltage saturation to ensure consistent performance across the operating range. The impact of each of these parameters on the compensated open loop response is as follows:

- ω_c: Increasing ω_c leads to better dynamic performance and transient response. This comes at the cost of reduced phase margin and potential stability issues.
- M_f: Directly impacts stability and transient performance. Higher values increases damping whilst lower values increases risk of oscillatory behaviour.
- K_p: Produces an output proportional to error. Higher values improve the system's responsiveness but also increase the risk of overshoot and oscillations.
- K_i: Helps to address steady-state error by summing the error over time and applying corrections based on that error. High values of K_i may lead to overshoot and slower settling time due to integration errors.
- K_d: Predicts future errors by calculating the rate of change of error. Provides damping to smooth out a response and prevent the system from reacting too quickly. High values can lead to an overly sensitive controller.

The tuning procedure for the gain parameters is as follows:

1. Configure the controller for only the chosen gain. Minimise the effects of the other actions by setting their gain to zero. Initialise the gain to 1.
2. Gradually increase the gain until the system exhibits self-sustaining oscillations. Once these oscillations have been induced, reduce the gain to half of this value to reduce system aggressiveness.
3. Repeat this process for each unique gain action.

After applying this heuristic method, the gains are manually tweaked to achieve the final parameter values and the compensated open loop system is derived and depicted by Table 6 and Figure 2. The margin values for the open loop compensated system and its corresponding closed loop response are depicted by Table 5 and Figure 3. As depicted by Figure 3, both the linear and nonlinear systems achieve the performance requirements and validates the designed controller.

3.5 Digital Emulation of the Controller on the Linear Model

In this section, the continuous-time controller designed in Section 3.4 is emulated using both the Zero-Order Hold (ZOH) and Forward Euler methods for discretisation. At

Parameter	Value
G_m	11.95
P_m	57.55
ω_c	357.52

Table 5: Compensated Open Loop Margin Values

Parameter	Value
ω_c	15
M_f	70°
K_p	2
K_i	75
K_d	40

Table 6: Controller Parameters

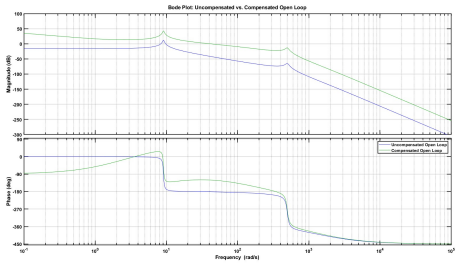


Figure 2: Uncompensated vs Compensated Open Loop Bode Plots

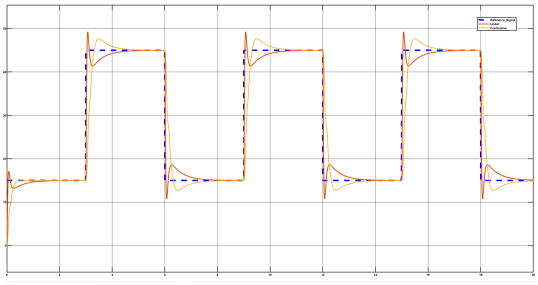


Figure 3: Linearised vs Nonlinear System Response

100Hz and 75Hz, both discretised controllers demonstrate a stable response to the step input, exhibiting similar behaviour as shown 4. Both systems achieve the steady-state error and settling time performance requirements at both sampling frequencies, however, both systems showed marginally degraded performance, with noticeable oscillations. However, the Euler discretisation at 100Hz and 75Hz achieves the overshoot/undershoot specifications whilst the ZOH discretisation does not. For both discretised systems, a critical observation is the onset of instability in the closed-loop behaviour as the sampling frequency decreases. Specifically, the closed-loop system becomes unstable at lower sampling frequencies, notably at 72 Hz for the Euler method and 62Hz for the ZOH method. These plots are depicted below in Figures 5 and 6. This worse performance at lower frequencies at can be explained by the following reasons:

- Since Euler method assumes linearity over each sampling interval, this leads to significant errors as the sampling frequency decreases.
- Euler method introduces delays that become more pronounced at lower sampling frequencies, further degrading performance.
- The errors accumulated by the Euler method accumulate more rapidly over time, causing the system to deviate from the desired behaviour. This is especially pronounced at lower sampling frequencies.

Moreover, when inspecting the pole-zero map of both isolated controllers, while the Euler discretised controller becomes unstable at 72Hz, the ZOH system always remains

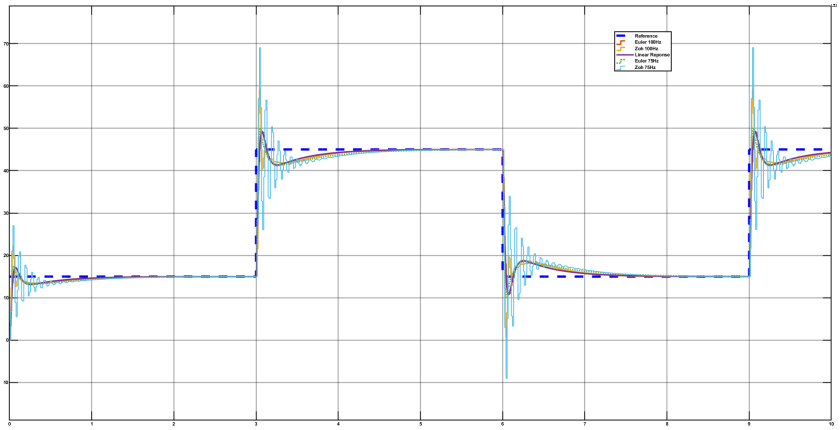


Figure 4: Discretisation at both 100Hz and 75Hz

stable, even for low frequencies. Figures 7 and 8 depict this described behaviour. A potential reason is that, the linearised plant could have dynamics that interact poorly with the controller. Alternatively, the sampling period could have introduced additional dynamics.

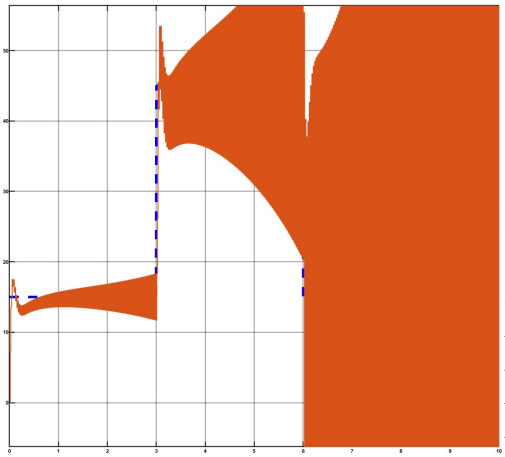


Figure 5: Euler Controller Unstable

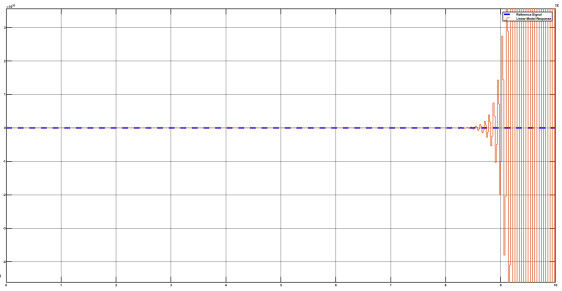


Figure 6: ZOH Controller Unstable

3.6 Implementation and Testing

3.6.1 Initial Implementation

As observed in Section 3.5, the Euler emulated controller in isolation is unstable at 72Hz. Therefore, a ZOH emulated controller using a sampling frequency of 50Hz is implemented. The initial implementation is depicted below in Figure 9. For reference, the performance of the same controller but in continuous time is plotted against it.

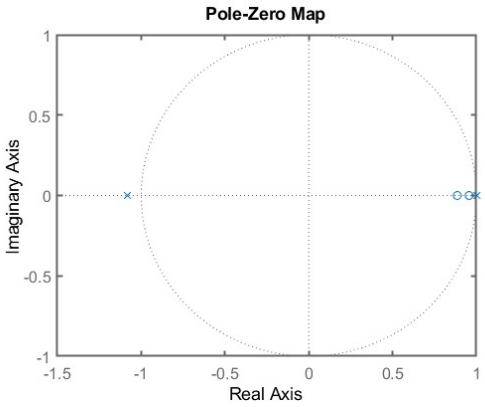


Figure 7: Euler Method at 72Hz

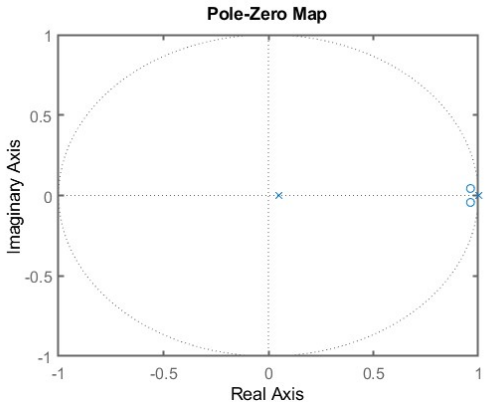


Figure 8: ZOH Method at 50Hz

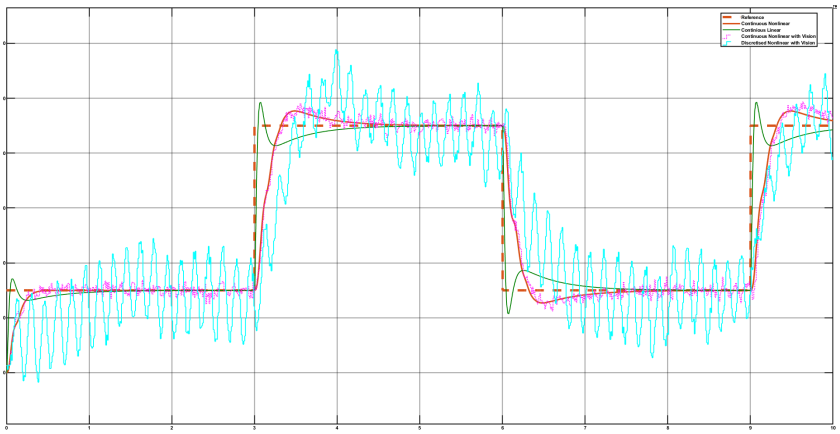


Figure 9: Initial Implementation of Emulated Controller

Whilst the discrete system tracks the reference signal, it does not meet the performance requirements, with substantial overshoot and oscillations present. To address these issues, the PID gains can be altered.

3.6.2 Redesign and Implementation

To address the oscillations and overshoot present in the current response, K_d and K_i were manually tuned downwards until the nonlinear plant fulfilled the performance requirements. The gains were tuned to $K_d = 10$ and $K_i = 25$. The impact of these changes is depicted below in Figures 10 and 11. It is worth noting that both the continuous and discrete linearised model responses do not meet the performance requirements whilst the nonlinear model responses meet such specifications. Additionally, the continuous time systems react more sluggishly.

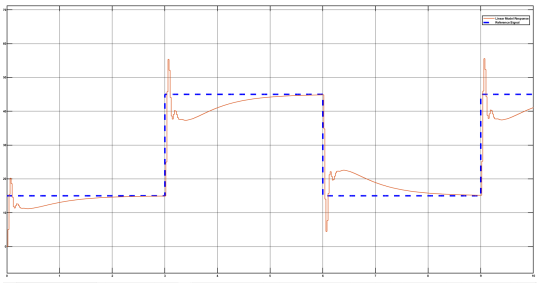


Figure 10: Tuned Emulated Controller on Linear Model

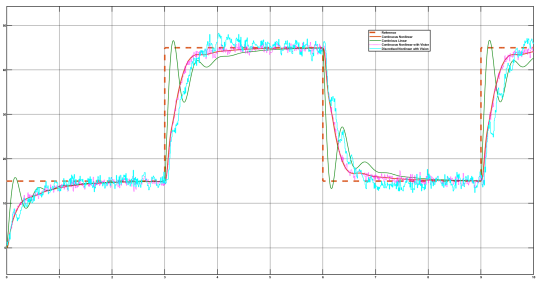


Figure 11: Tuned Emulated Controller on Nonlinear Model

4 Discussion

One key observation made when initially implementing the discretised controllers was the increase in oscillatory behaviour exhibited by the closed-loop response. This behaviour is also observed when implementing the digital sensor. In both instances, this can be attributed to the derivative action of the PID controller. As stated in Section 3.4, derivative action computes the rate of change of the error signal and provides a correction based on this rate of change.

When applied to a discrete model, the discrete derivative approximation can be very sensitive, as the discrete differences between the sampled points used to calculate the rate of change can be exacerbated, depending on sampling frequency. Reducing this gain action was demonstrated to reduce oscillations and improve performance as per Section 3.6. Moreover, Motor 2 having an innately fast response due to its high angular velocity could have also exaggerated this problem. This could be addressed by using Motor 1 instead, since it should offer better precision with its high torque and should not respond as fast to inputs.

Although the controller was designed using the linear model, it performed differently on the nonlinear system potentially due to unmodeled dynamics like actuator nonlinearity. In future projects, incorporating estimation methods, such as observers or filters, can improve control accuracy by providing estimates of unmeasured states, leading to more precise and robust system performance.

5 Conclusion

The performance objectives for this project were only partially meet. While the nonlinear model did eventually meet the performance specifications after some tuning, the linear model did not. Key insights include the impact of sampling frequency and discretisations. Additionally, the importance in understanding the limitations of linearised models and an emphasis on robust controller design were also heavily underscored.